STEEL SEVIER

Contents lists available at ScienceDirect

# International Journal of Biological Macromolecules

journal homepage: http://www.elsevier.com/locate/ijbiomac



# Preparation and characterization of rod-like chitosan–quinoline nanoparticles as pH-responsive nanocarriers for quercetin delivery



Shahnaz Rahimi, Sepideh Khoee \*, Mehdi Ghandi

School of Chemistry, College of Science, University of Tehran, PO Box 14155 6455, Tehran, Iran

#### ARTICLE INFO

Article history: Received 4 October 2018 Received in revised form 10 January 2019 Accepted 24 January 2019 Available online 26 January 2019

Keywords: Chitosan 2-Chloro-3-formylquinoline 3-Formylquinolin-2(1H)-one Nanorod shape Drug delivery system

#### ABSTRACT

Novel chitosan–quinoline nanoparticles as anticancer drug nanocarriers were prepared using 2-chloro-3-formylquinoline and 3-formylquinolin-2(1H)-one as non-toxic modifying agents via oil–in–water nanoemulsion technique. Chitosan–quinoline nanoparticles were characterized by FT–IR, UV–vis spectrophotometry, XRD, SEM, AFM and DLS techniques. The morphological and particle size studies demonstrated that drug–loaded chitosan–quinoline nanoparticles have a regular nanorod shape and monolithic structure with the desired particle size of 141 to 174.8 nm and a negative zeta potential of -2.4 to -14.1 mV. Drug loading capacity (LC) and encapsulation efficiency (EE) were achieved using quercetin as a hydrophobic anticancer drug and were about 4.8–9.6% and 65.8–77%, respectively. The in vitro release studies displayed great pH-sensitive release behavior. Evaluation of the anticancer efficacy of quercetin loaded chitosan–quinoline nanoparticles using the in vitro cytotoxicity studies against HeLa cells indicated that the chitosan nanoparticles are a promising candidate for the anticancer drugs delivery.

 $\ensuremath{\mathbb{C}}$  2019 Elsevier B.V. All rights reserved.

## 1. Introduction

Chitosan is a natural biopolymer generally produced by deacetylation of chitin with excellent accessibility, biodegradability, biocompatibility, nontoxicity and antimicrobial activity [1]. Chitosan has been extensively used as a material in numerous biomedical and pharmaceutical fields, such as gene delivery, biosensors, tissue engineering and drug delivery systems. Chitosan and its derivatives have received the most attention among researchers owing to its various physicochemical features and biological activities [2–6]. Due to its excellent adhesion property, chitosan can enhance the cell membrane permeability [7]. Accordingly, various drug carriers are designed using chitosan and its derivatives. Fu et al. developed chitosan hollow microspheres (CHM) as a new carrier for tough hydrophobic drugs based on an interfacial Schiff-base bonding reaction [8]. Liu et al. designed monodisperse core-shell chitosan microcapsules via a crosslinking reaction of O/W/O double emulsion of chitosan and terephthalaldehyde, which exhibited a pH-responsive burst release of hydrophobic drugs [9]. These findings show that chitosan and its derivatives are suitable candidates for drug carriers. However, concerns about the safety of chitosan particles remains owing to the toxicity of organic crosslinking agents especially glutaraldehyde, which causes adverse effects on the human body [10,11]. Natural and non-toxic products possessing biological properties can be used as crosslinking agents to overcome the potential side effects. Therefore, the choice of the appropriate crosslinking agent is a novel and interesting challenge for the preparation of chitosan nanoparticles [12,13].

Quinolines are important biological compounds because of their occurrence in a large number of natural products especially in alkaloids, and their broad range of applications in pharmaceuticals, medicine and agrochemicals [14,15]. Due to their good efficacy and desirable safety profiles, compounds containing quinoline have attracted considerable attention for their diverse bioactivities like antifungal [16], antiinflammatory [17.18], antimalarial [19], antiviral [20], antimicrobial [21,22], anticancer [23,24] and analgesic activities [18]. Moreover, quinoline and its derivatives have been widely utilized in medicinal chemistry due to the occurrence of their structure in the number of commercial drugs such as mefloquine [25], quinine [26], amodiaquine [27] and chloroquine [28]. Among the quinoline derivatives, 2,3-disubstituted quinolines and 3-substituted quinolin-2-ones have played an important role in the design and development of novel compounds with marvelous anticancer activities [29,30]. Inspired by the known properties of quinoline and its derivatives, we undertook a study for the synthesis of novel drug-loaded chitosan-quinoline nanoparticles with 2-chloro-3formylquinoline (CFQ) and 3-formylquinolin-2(1H)-one (FQO) as non-toxic modifying agents via oil-in-water (O/W) nanoemulsion method. The obtained chitosan-quinoline nanoparticles were characterized by means of FT-IR, XRD, UV-vis, SEM imaging techniques and other spectroscopic methods. Quercetin was loaded into the modified chitosan nanoparticles as a model anticancer drug. Furthermore, the

<sup>\*</sup> Corresponding author.

E-mail addresses: Khoee@khayam.ut.ac.ir (S. Khoee), ghandi@khayam.ut.ac.ir (M. Ghandi).

**Table 1**Diffusion exponent and solute release mechanism for rod shape matrices.

Diffusion exponent (n)	Overall solut diffusion mechanism			
n < 0.45 0.43 < n < 0.89	Fickian diffusion Anomalous (non-Fickian) diffusion			
0.89 < n < 1	Case II transport			
n > 1	Super case II transport			

release of quercetin from the chitosan-quinoline nanoparticles was evaluated and cytotoxicity against HeLa cells was also investigated using MTT assay.

## 2. Experimental

## 2.1. Materials

Chitosan (CS) with low molecular weight (MW = 50,000-190,000 Da, degree of deacetylation: 85%), Dulbecco's Modified Eagle's medium (DMEM) and 3-(4,5-dimethylazolyl-2)-2,5-diphenyl tetrazolium bromide (MTT) were purchased from Sigma-Aldrich. Quercetin was purchased from Fluka Chemical Co. Phosphoryl chloride (POCl<sub>3</sub>), *N,N*-dimethylformamide (DMF), acetanilide, glacial acetic acid (CH<sub>3</sub>COOH, 100%), Tween 60 (polyoxyethylene sorbitan monostearate, HLB = 14.9), dichloromethane (CH<sub>2</sub>Cl<sub>2</sub>, 99%), ethanol (EtOH, 99%) and other commercially available chemicals were supplied from Merck Chemical Company and used without further purification.

### 2.2. Measurements

The <sup>1</sup>H NMR of the organic products was recorded on a Bruker 500 MHz NMR spectrometer using CDCl<sub>3</sub> as the solvent at 25 °C. Melting points were carried out by an Electrothermal model 9100 apparatus and are uncorrected. Mass spectra of the organic compounds were obtained using an HP (Agilent technologies) 5937 Mass Selective Detector. Fourier transform infrared (FT-IR) spectra were performed in KBr pellets by FT-IR spectrophotometer (IR Affinity, Shimadzu, Japan) using KBr in the range of 600-4000 cm<sup>-1</sup>. The average particle size and zeta potential of the chitosan-quinoline nanoparticles were determined by dynamic light scattering (DLS, Brookhaven instrument, USA) at 25 °C in triplicate. Each sample was diluted to the desired concentration using deionized water and the analysis was carried out at a fixed scattering angle of 90°. Ultraviolet-visible (UV-vis) absorption spectra were determined on a UV-vis spectrophotometer (Jasco V750, Jasco, Tokyo, Japan). The shape of the obtained nanoparticles was analyzed by scanning electron microscopy (FE-SEM) (HITACHI S-4160, Japan). Samples were mounted on an aluminium stub using a double adhesive carbon tape and then sputtercoated with gold before observations. X-ray diffraction (XRD) analysis of the samples was conducted by an X-ray diffractometer (Rigaku, Japan) with  $CuK\alpha$  radiation as target. The measurement was carried out at a voltage of 40 kV and 40 mA current and 20 angle range from 5° to 50° at a scanning speed of 4° min<sup>-1</sup> at room temperature. The topography of the drug-loaded chitosan-quinoline nanoparticles was characterized by atomic force microscopy (AFM, ENTEGRA AFMNT-MDT, China) on a freshly cleaved mica substrate.

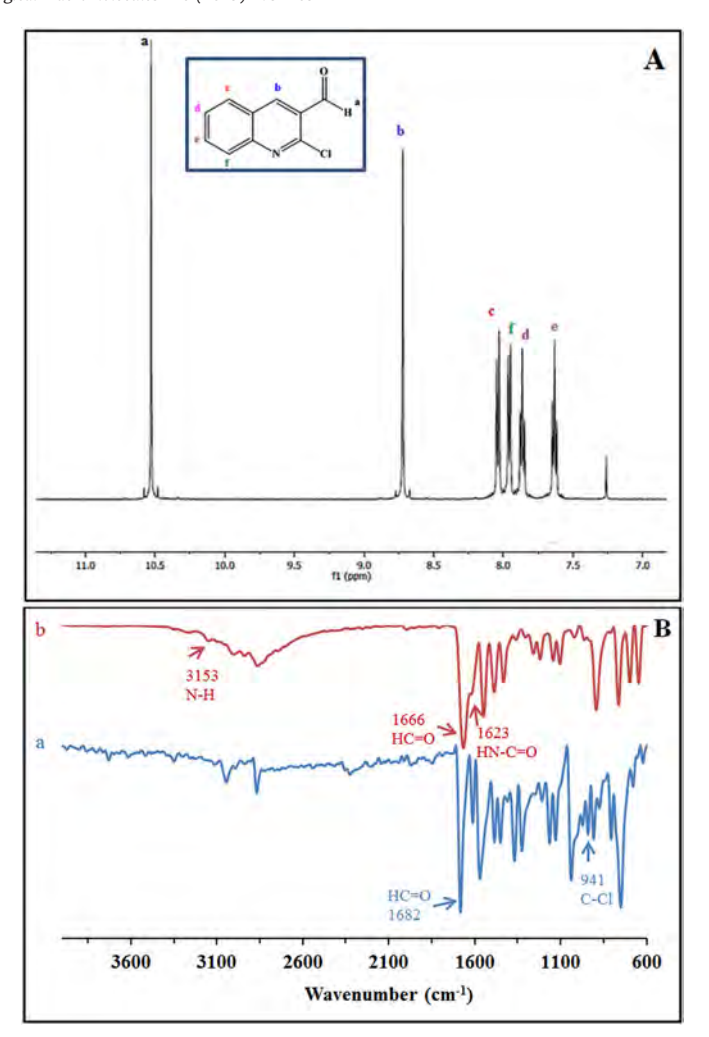


**Fig. 1.** (A) <sup>1</sup>H NMR spectra of CFO and (B) FT-IR spectra of CFO (a) and FOO (b).

## 2.3. Synthesis and characterization of 2-chloro-3-formylquinoline

Dry DMF (2.7 mL, 34.65 mmol) was cooled to 0–5 °C in a round bottom flask, and POCl<sub>3</sub> (9 mL, 98.28 mmol) was added dropwise by a dropping funnel to DMF with stirring. After stirring the solution for about 15 min, acetanilide (1.4 g, 10.37 mmol) was added and the mixture heated at 75–80 °C for 8 h. The reaction mixture was then poured into crushed ice under vigorous stirring for about 30 min. The precipitate thus appeared was filtered, washed well with cold water and dried. Recrystallization of the crude compound from ethyl acetate finally afforded the product 1 in high yield (90%), mp: 147–148 °C; FT–IR (KBr),  $\nu$ , cm<sup>-1</sup>: 1682 (HC=O), 943 (C—Cl); ¹H NMR (500 MHz, CDCl<sub>3</sub>):  $\delta$  7.61 (t, J = 7.3 Hz, 1H), 7.86 (t, J = 7.3 Hz, 1H), 7.95 (d, J = 8.1 Hz, 1H), 8.04 (d, J = 8.1 Hz, 1H), 8.72 (s, 1H), 10.52 (s, 1H); ESI–MS m/z: [M + H]<sup>+</sup>calcd. for C<sub>10</sub>H<sub>6</sub>CINO = 191.01; found 191.3 (Fig. S1).

Scheme 1. Synthesis of CFQ e and FQO.

## 2.4. Synthesis and characterization of 3-formylquinolin-2(1H)-one

A suspension of 2-chloro-3-formylquinoline (1 mmol) in acetic acid (70%, 10 mL) was stirred under reflux for 4–6 h. After completion as indicated by TLC, the reaction mixture was cooled to room temperature and the precipitated product filtered, washed with water and dried. (yield 93%; mp: 302–303 °C); FT–IR (KBr),  $\nu$ , cm<sup>-1</sup>: 3153 (N—H), 1666 (HC=O), 1623 (NHC=O);  $^1$ H NMR (500 MHz, CDCl<sub>3</sub>):  $\delta$  7.72 (t, J = 7.1 Hz, 1H), 7.93 (t, J = 7.1 Hz, 1H), 8.05 (d, J = 8.3 Hz, 1H), 8.14 (d, J = 8.3 Hz, 1H), 8.76 (s, 1H), 10.27–10.48 (br s, 1H), 10.63 (s, 1H); ESI-MS m/z: [M + H] $^+$ calcd. for C<sub>10</sub>H<sub>7</sub>NO<sub>2</sub> = 173.1; found 173.0 (Fig. S2).

## 2.5. Preparation of chitosan-quinoline nanoparticles

Chitosan–quinoline nanoparticles were prepared via the O/W nanoemulsion system. Briefly, chitosan (1%, w/v) was dissolved in dilute acetic acid solution (0.7%, v/v) at ambient temperature and vigorously stirred overnight (1400 rpm). After addition of Tween 60 (1%, w/v), the mixture was sonicated in an ultrasonic probe for 15 min until the aqueous phase mixture became homogeneous. Ouercetin was dissolved in

EtOH-CH<sub>2</sub>Cl<sub>2</sub> solution (1:3, v/v) to obtain a final concentration of 10% (w/w of chitosan) and stirred for 10 min until the oil phase mixture became transparent. Thereafter, the oil phase was added dropwise into the aqueous phase and sonicated for 5 min to form O/W emulsion. The volume ratio of O/W was fixed at 1:5. Afterwards, a solution of quinoline derivatives (0.5%, w/v) as the modifying agents was poured into the O/W nanoemulsion dropwise to prepare the crosslinked chitosan–quinoline nanoparticles suspension. The crosslinked chitosan nanoparticles solution was then centrifuged at 16,000 rpm for 30 min at 20 °C. Finally, the obtained chitosan–quinoline nanoparticles were washed well with deionized water and freeze–dried for 12 h (Tajhizat Sazan Pishtaz, Iran). The blank chitosan–quinoline nanoparticles prepared similarly without adding of quercetin.

## 2.6. Drug loading and encapsulation efficiency

The encapsulation efficiency (EE) and loading capacity (LC) of quercetin loaded in chitosan–quinoline nanoparticles were determined by centrifugation of the drug–loaded chitosan–quinoline nanoparticles at 16,000 rpm for 30 min to remove the non–entrapped quercetin. The clear supernatant was analyzed to measure the ultraviolet absorbance

## Chitosan-quinoline nanoparticles

Scheme 2. Synthesis of chitosan-quinoline nanoparticles modified with CFQ (A) and with FQO (B).

by using a UV–vis spectrophotometer at 373 nm. EE and LC were thus estimated from Eqs. (1) and (2), respectively:

$$EE(\%) = \frac{QCt - QCf}{QCf} \times 100 \tag{1}$$

$$LC(\%) = \frac{QCt - QCf}{Weight \ of \ nanoparticles} \times 100 \tag{2}$$

where QCt is the total amount of quercetin used in the preparation of nanoparticles and QCf is the free quercetin present in the supernatant.

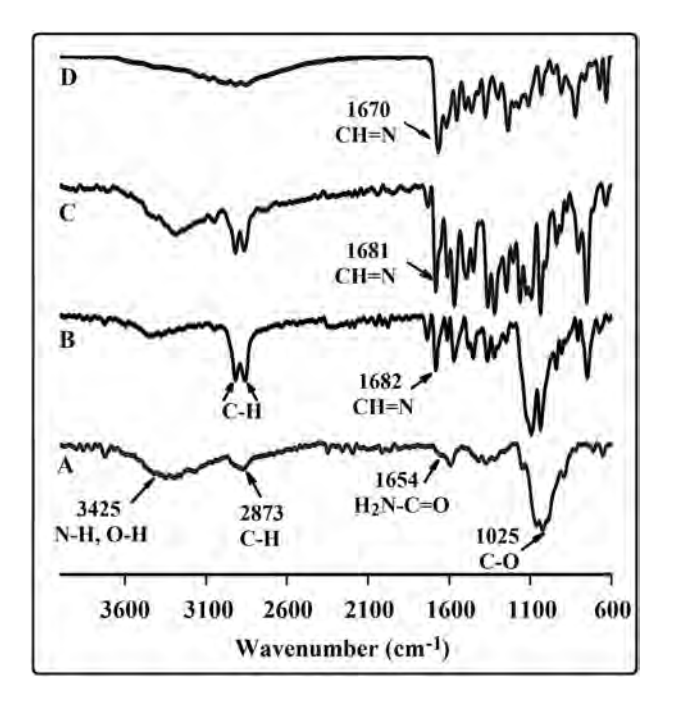
#### 2.7. In vitro quercetin release

The quercetin release profile of the chitosan-quinoline nanoparticles was carried by a dialysis method. Typically, the weighed freeze-dried quercetin-loaded chitosan-quinoline nanoparticles were dispersed in release medium (phosphate buffer saline (PBS), pH 7.4 and pH 5.8) with a concentration of 1 mg/mL at a membrane dialysis bag (cut off 12,000 kDa). The end-sealed dialysis bag was suspended into a container with 10 mL of PBS at the same pH value as that in the bag. The outer phase of the release media was maintained at 37  $\pm$  0.5 °C with continuous stirring at a speed of 50 rpm. At prescheduled time intervals, 5 mL of samples were withdrawn in both of pH medium and replaced with an equal volume of fresh media to maintain a constant volume. The cumulative amount of guercetin released from chitosan-guinoline nanoparticles in each buffer was determined by measuring the absorbance at 373 nm in a UV-vis Spectrophotometer. To identify the mechanism for the release of quercetin from crosslinked and non-crosslinked chitosans, the suitability of Higuchi [31] and Korsmeyer-Peppas [32] equations were evaluated according to the following equations (Eqs. (3) and (4), respectively):

$$\frac{M_t}{M_\infty} = k\sqrt{t} \tag{3}$$

$$\frac{M_t}{M_\infty} = k't^n \tag{4}$$

where, Mt is cumulative amounts of released drug at time t and  $M \infty$  is cumulative amounts of released drug at infinite time. K and k' are Higuchi



 $\label{eq:Figeneral} \textbf{Fig. 2.} \ FT\text{-IR spectra of the pure chitosan (A), blank chitosan-quinoline nanoparticles (B) and drug-loaded chitosan-quinoline nanoparticles crosslinked with CFQ (C) and FQO (D).$ 

and Korsmeyer–Peppas constant. In the case of rod shape polymeric vehicles, n values that are used as release mechanism characterization are listed in Table 1.

## 2.8. In vitro cytotoxicity evaluation

MTT assay using HeLa cell lines was employed for determination of the in vitro cytotoxicity of free quercetin and the quercetin-loaded chitosan-quinoline nanoparticles. Typically, HeLa cells were seeded into 96-well plates at the density of  $1.25 \times 10^4$  cells per well in 180 µL DMEM and then incubated in humidified incubator of 5% CO<sub>2</sub> at 37 °C for 24 h. After that, the medium was replaced by fresh corresponding medium containing solutions of pure quercetin and drug-loaded chitosan-quinoline nanoparticles at concentrations of 10 to 400  $\mu g \text{ mL}^{-1}$ . After incubated for 48 h, 20  $\mu L$  of MTT solution (5  $\mu g \text{ mL}^{-1}$  in PBS) was added to every well and the cells were incubated for another 4 h. The medium containing MTT was then removed, and displaced by 150 µL of dimethyl sulphoxide (DMSO) per well for 10 min at ambient temperature to dissolve the formazan crystals. Finally, the absorbance of the solution was measured at a wavelength of 570 nm using a microplate reader and the relative cell viability (%) was calculated by the following equation:

$$Cell\ viability(\%) = \frac{Abs(test\ cell)}{Abs(controlled\ cell)} \times 100\% \tag{3}$$

## 2.9. Optical microscopy analysis

HeLa cells were cultured in 24-well plates at a density of  $1 \times 10^4$  cells per well. After 24 h of incubation, cells were incubated without

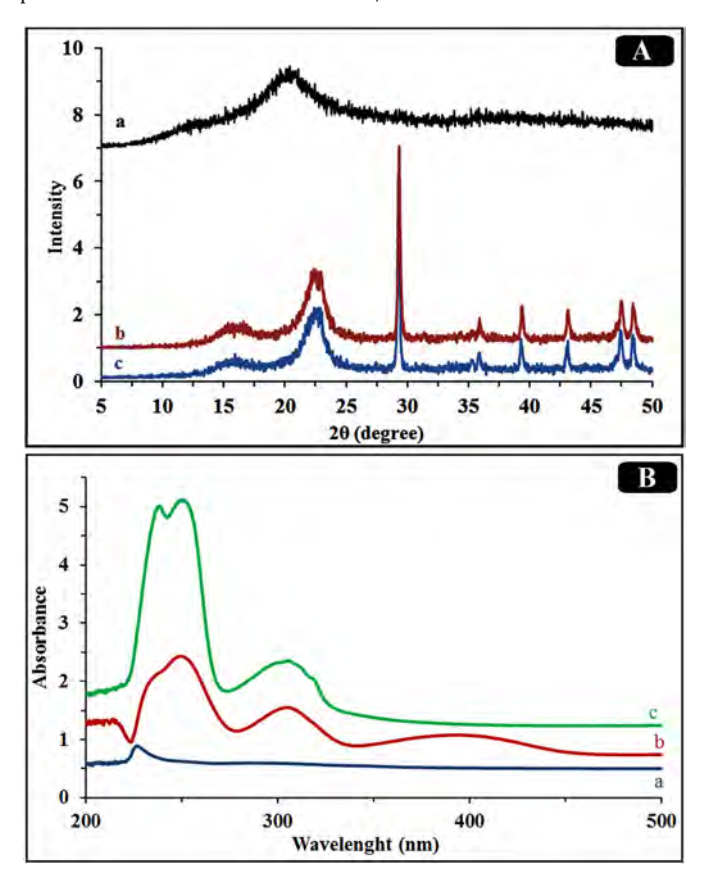


**Fig. 3.** A: XRD patterns of chitosan powder (a), drug–loaded chitosan nanoparticles crosslinked with FQO (b) and drug–loaded chitosan nanoparticles crosslinked with CFQ (c). B: UV–vis spectra of the pure chitosan (a), chitosan nanoparticles crosslinked with FQO (b) and chitosan nanoparticles crosslinked with CFQ (c).

nanoparticles as control or with different concentration (100, 200 and 400  $\mu g \ mL^{-1}$ ) of two types of chitosan nanorods for 4 h at 37 °C. After that, morphologies of the cells were observed using an optical microscope.

## 3. Results and discussion

## 3.1. Design, synthesis and characterization

CFQ and FQO were prepared according to the procedure previously reported [30,33] as the modifying agents for the preparation of chitosan-quinoline nanoparticles. The synthetic routes are presented in Scheme 1. CFQ was synthesized starting from acetanilide via a Vilsmeier–Haack reaction. Subsequently, heating CFQ in aqueous acetic acid at reflux led to FQO in good yield (93%). All spectral data including IR, <sup>1</sup>H NMR and Mass of 2-chloro-3-formylquinoline and 3-formylquinolin-2(1*H*)-one were consistent with those of authentic samples.

The  $^{1}$ H NMR spectrum of CFQ revealed characteristic signals at  $\delta$  10.52 (s, 1H) and 7.61–8.04 (m, 5H) due to the aldehyde and aromatic protons, respectively (Fig. 1A).

Similarly, the appearance of signals at  $\delta$  10.27–10.48 (brs, 1H), 10.63 (s, 1H) and 7.72–8.76 (m, 5H) due to the NH, aldehyde and aromatic protons in the  $^1$ H NMR spectrum of FQO is consistent with the suggested structure (Fig. S3). The IR spectrum of CFQ exhibited the main signals at 1682 cm $^{-1}$  and 941 cm $^{-1}$  for C=O and C-Cl, respectively. The most prominent signals in the IR spectrum of FQO corresponded to the intense absorption bands at 3153 and 1666–1623 cm $^{-1}$  attributed to the amide NH and carbonyl groups together with the disappearance of signal at 941 cm $^{-1}$  for C-Cl absorption (Fig. 1B).

The chitosan–quinoline nanoparticles were prepared by Schiff base reaction of the chitosan chains amine and the quinoline aldehyde groups (Scheme 2). Moreover, the chitosan–quinoline nanoparticles are further stabilized through the formation of hydrogen bonding between FQO amide groups. This in turn enhances the physicochemical properties of chitosan–quinoline network. On the other hand, because of the biological activity of quinoline compounds and their non-

toxicity properties, it is expected that the incorporation of quinoline into chitosan polymer furnishes novel nanoparticles with modified biological activity.

The FT–IR spectra of pure chitosan and chitosan–quinoline nanoparticles are presented in Fig. 2. The pure chitosan spectrum reveals the absorption peaks in 3200–3600, 3425 and 2873 cm<sup>-1</sup> due to the intra-and intermolecular different –OH hydrogen bonds, N—H/O—H, and C—H stretching vibrations, respectively. Whereas other characteristic peaks of chitosan appears at 1654, 1592 and 1375 cm<sup>-1</sup> are assigned to the amide I C=O, amide II NH and amide III NHCO stretching vibrations, respectively, the broad peak displayed at 1025 cm<sup>-1</sup> was attributed to the C—O absorption [34,35].

Compared to the pure chitosan, the strong absorption peaks observed at 1682 and 1670 cm<sup>-1</sup> in the spectrum of the chitosan-quinoline nanoparticles due to C=N stretching vibrations indicate that imine bond formation has occurs via a chemical modification between the chitosan chains amine and quinoline aldehyde groups [36,37]. Other specific peaks displayed at 752, 815, 1451 and 1612 cm<sup>-1</sup> are attributed to the quinoline aromatic ring. Finally, observation of an increase in the absorptions at 2864 and 2918 cm<sup>-1</sup> concomitant with the omission of absorbance at 2000–3900 cm<sup>-1</sup> is significant, perhaps due the formation of chitosan–quinoline nanoparticles.

The XRD spectrum of pure chitosan presented in Fig. 3A revealed the two broad peaks at  $2\theta=12$  and  $20^\circ$  in the former and in agreement with the previous reports [38]. In the XRD patterns of drug–loaded chitosan–quinoline nanoparticles, diffractive region is observed at  $2\theta$  of 16, 22, 29, 36, 39, 43, 47, and  $48^\circ$ . Observation of higher intensity in the XRD pattern of drug–loaded chitosan nanoparticles crosslinked with quinoline derivatives indicates their more crystalline structure. As such, it can be concluded that chemical modification with quinoline derivatives has converted the amorphous chitosan nanoparticles into a crystalline form.

The UV-vis absorption spectra of pure chitosan and chitosan-quinoline particles at 25 °C are shown in Fig. 3B. Whereas the UV-vis absorption spectrum of pure chitosan is transparent and shows only a weak absorption band at 224 nm, those for chitosan-quinoline particles

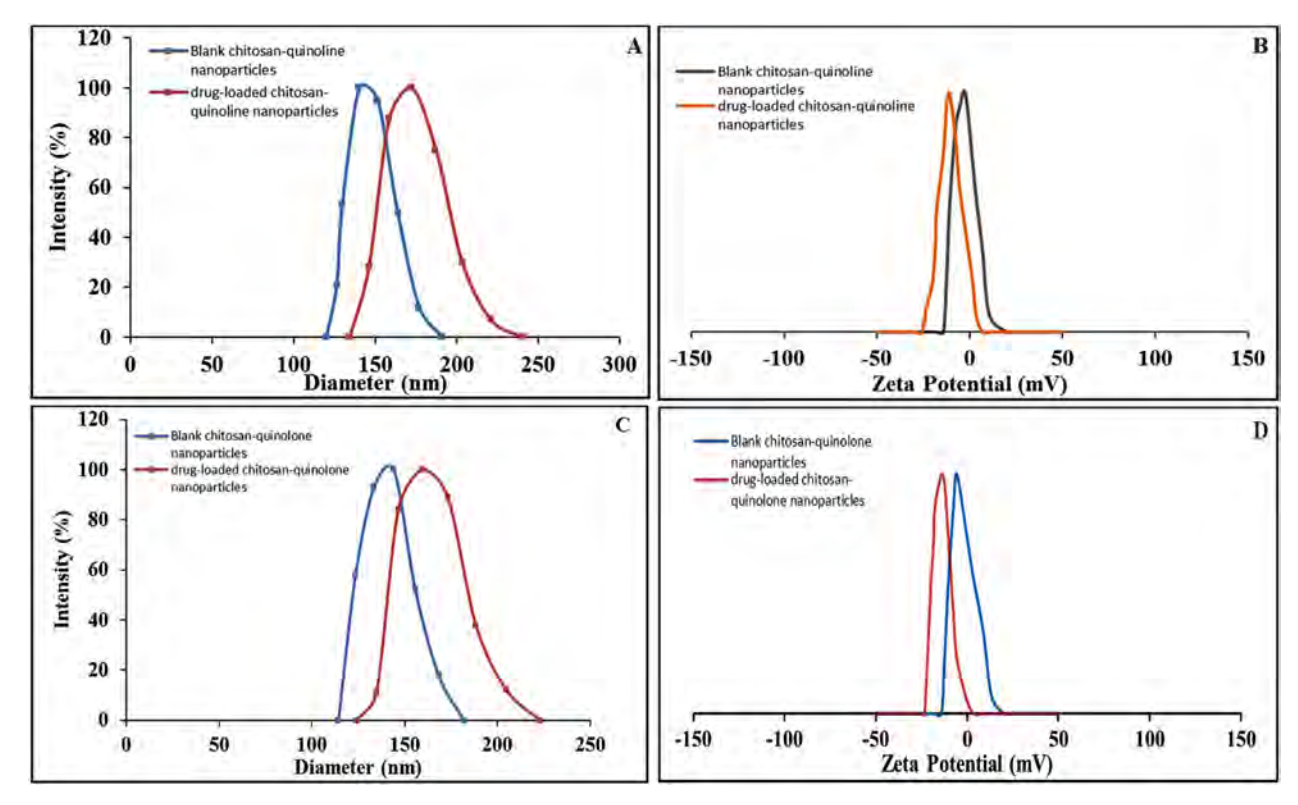


Fig. 4. DLS results of chitosan nanoparticles crosslinked with CFQ (A) and FQO (C), and their zeta potential results: CFQ (B) and FQO (D).

indicate two maxima at 250 and 306 nm due to the existence of  $\pi \to \pi^*$  and  $n \to \pi^*$  transitions of the azomethine chromophore moiety and quinoline heterocyclic ring. In addition, the UV–vis absorption spectrum of chitosan particles crosslinked with FQO exhibited a broad absorption band between the 360–450 nm regions, which could be assigned to the amide delocalized  $\pi$ -bond.

The particle size of the chitosan–quinoline nanoparticles was determined by dynamic light scattering (DLS) technique. Because of the adhesion property of chitosan in aqueous solution, the nanoparticles tend to produce aggregates, which lead to an increase in their average hydrodynamic diameter [39]. The progressive dispersion of the nanoparticles in aqueous suspension has been suggested as an efficient method of decreasing the inter-particle interactions [40] and utilized in this research. As indicated in Fig. 4A and B, the average diameter of 150.7 nm with a zeta potential of -2.4 mV of blank chitosan nanoparticles crosslinked with CFQ changes to 174.8 nm with a zeta potential of -10.8 mV upon loading of quercetin. Accordingly, the average diameter of 141.2 nm with a zeta potential of -5.7 mV of the blank chitosan nanoparticles crosslinked with FQO also changes to 165.1 nm with a zeta potential of -14.1 mV upon loading of quercetin (Fig. 4C and D). As such, the suitability of the chitosan-quinoline nanoparticles with negative zeta potential values as a drug delivery system is concluded.

The characterization of morphology and topography of the chitosan–quinoline nanoparticles was carried out using SEM and AFM techniques. The SEM images of blank and quercetin–loaded chitosan nanoparticles crosslinked with quinoline derivatives presented in Fig. 5 reveals that the blank chitosan–quinoline nanoparticles have

spherical shape and nanosize structure, also reveal nearly uniform distribution with no intense particle agglomeration.

The morphology of quercetin–loaded chitosan nanoparticles crosslinked with CFQ is a monolithic structure with a kind of pattern and the morphology of quercetin–loaded chitosan nanoparticles crosslinked with FQO is nanorod structure along with uniformity in size (Fig. 5C–F). Differences in the morphology of the blank chitosan–quinoline nanoparticles and quercetin–loaded chitosan–quinoline nanoparticles can be attributed to the intermolecular hydrogen bonding and  $\pi$ – $\pi$  ( $\pi$ –stacking) interactions present between quercetin and quinoline derivatives (Scheme S1).

In addition, AFM topographic images and 3D models of the surface topography (Fig. 6) confirmed the nanorod-like morphology and nearly homogenous structure of quercetin–loaded chitosan nanoparticles made by crosslinking with quinoline derivatives, in agreement with SEM observations. The rod–like nanoparticles exhibited the enhanced cell adhesion, improved cell proliferation and transfection of living cells via their higher surface areas, with more effective penetration in tumors in comparison to those of spherical analogues [41]. Therefore, the quercetin–loaded chitosan nanoparticles crosslinked with quinoline derivatives having such surface morphology is favored for use in biomedical applications, especially drug delivery systems.

#### 3.2. Drug loading capacity and in vitro release profile

Quercetin, a potent and hydrophobic anticancer drug, was employed to measure the drug loading and release profile of the chitosan-

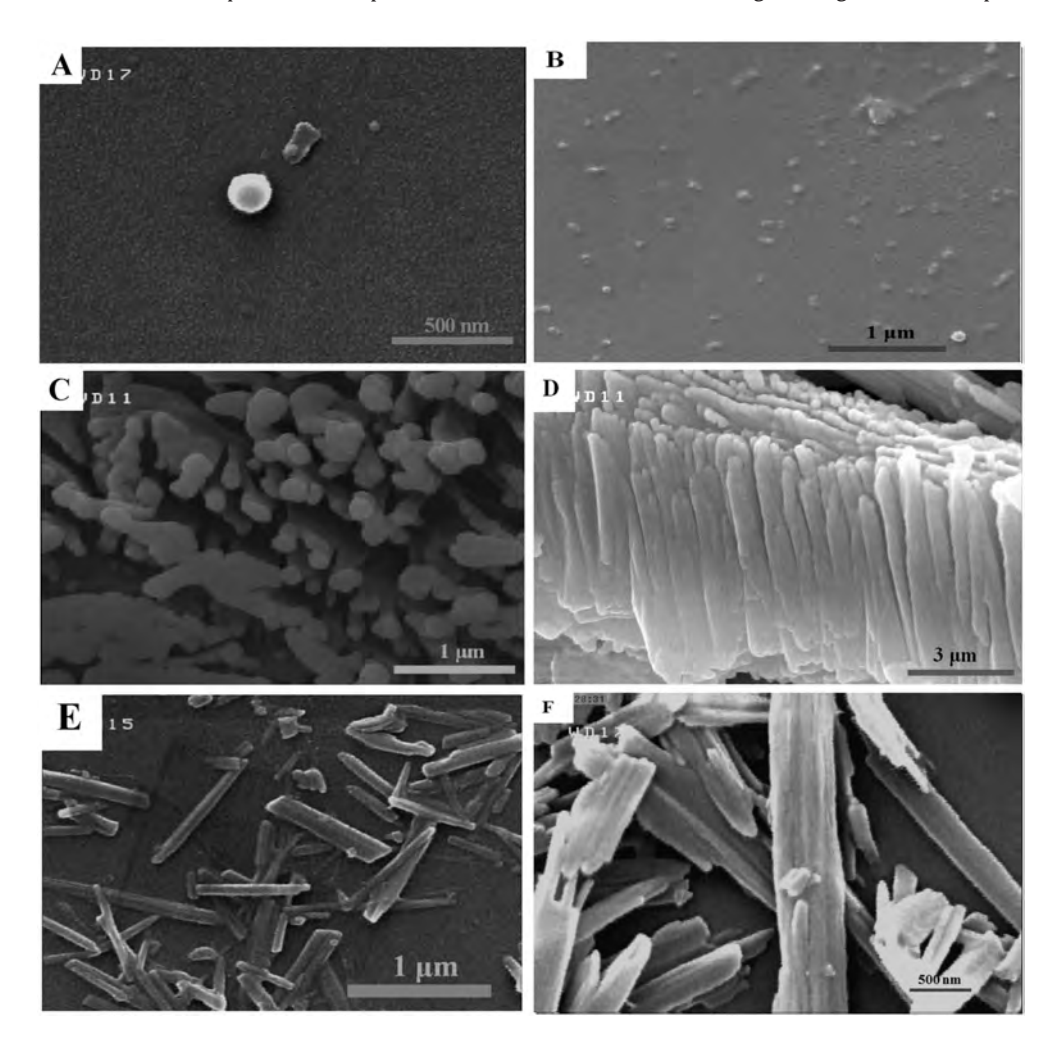


Fig. 5. SEM images of the blank chitosan nanoparticles crosslinked with CFQ (A), crosslinked with FQO (B), drug-loaded chitosan nanoparticles crosslinked with CFQ (upper surface (C) and side surface (D)) and crosslinked with FQO (E) and (F).

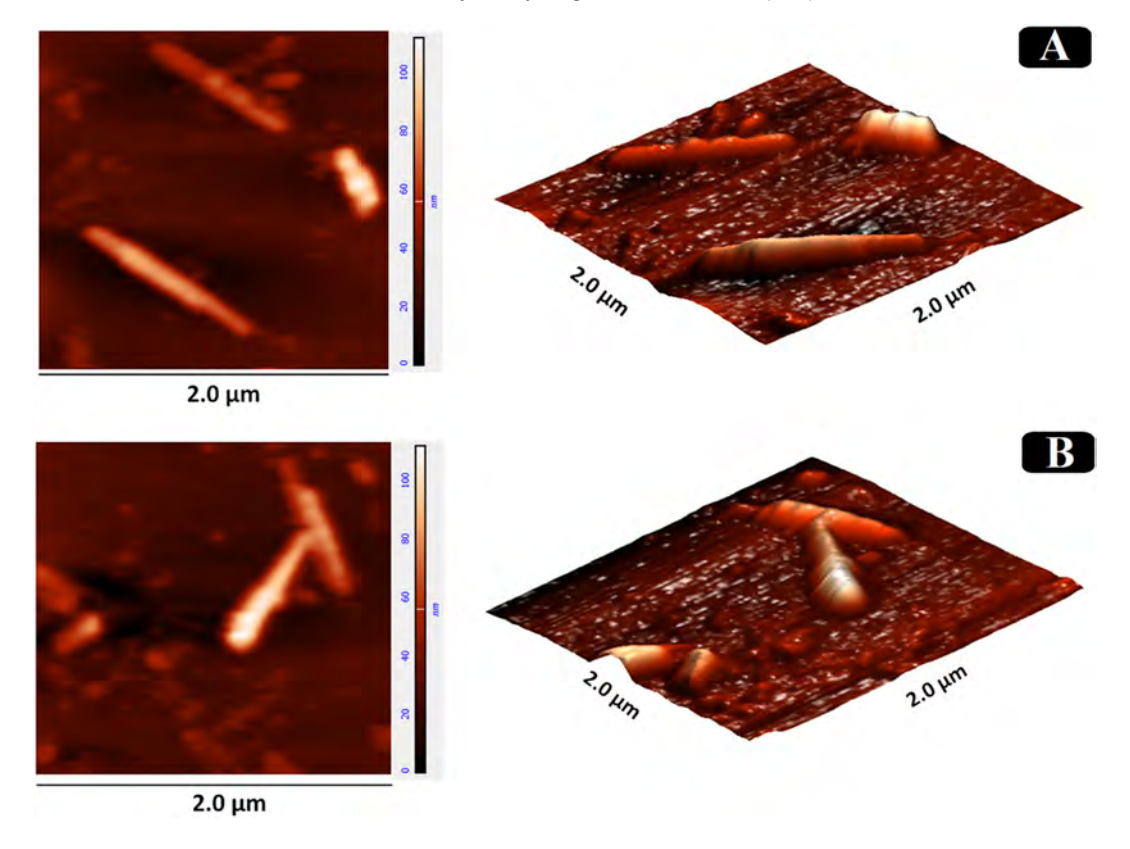


Fig. 6. AFM images (2D) and (3D) of drug-loaded chitosan nanoparticles crosslinked with CFQ (A) and drug-loaded chitosan nanoparticles crosslinked with FQO (B).

quinoline nanoparticles. Low encapsulation efficiency was not expected due to the hydrophobic and  $\pi$ - $\pi$  ( $\pi$ -stacking) interactions as well as intermolecular hydrogen bonding present between quercetin and the crosslinked chitosan nanoparticle quinoline groups. Accordingly, the drug LC and EE of the chitosan nanoparticles crosslinked with FQO determined as 9.6% and 77.2%, respectively, were higher than those of 4.8% and 65.8% found for chitosan nanoparticles crosslinked with CFQ. These efficiencies are higher than that found for quercetin-loaded chitosan nanoparticles modified with glycyrrhetinic acid [42]. The encapsulation efficiency depends on several parameters and one of the most important ones is the strong affinity between hydrophobic drug and hydrophobic domains in nanocarrier. It was found that these hydrophobic domains in chitosan could be obtained by adding hydrophobic comaterials to the carrier formulation, like lecithin [43], or pre-adhering of quercetin to carriers before particle crosslinking [44]. In this report, we used the former method, by inserting aromatic crosslinkers in the structure of chitosan. Consequently, a larger amount of quercetin preferred to encapsulate in nanocarriers during nanoparticle formation process. However, these interactions may reduce the diffusion of quercetin from nanocarriers during the release process. On the other hand, the low solubility of quercetin in water, automatically forced the drug molecules to attract to the surface or outer layers of nanoparticle and enhance its encapsulation efficiency. But, afterward, a complete release of drug in short period of time is observable in these systems. These results exhibit the improved stability of the quercetin-loaded chitosan nanoparticles crosslinked with FQO. The quercetin release profile of the chitosan-quinoline nanoparticles and chitosan nanoparticles without using quinoline derivatives in response to pH values of 7.4 and 5.8 was studied in a dialysis setup at 37 °C. Based on the in vitro release profile, it was found that the chitosan nanoparticles crosslinked with quinoline derivatives release quercetin much faster at pH 5.8 than that of pH 7.4. In acidic environment at low pH value (pH < 6), the amino groups of chitosan are protonated and positively charged, so its intramolecular electrostatic repulsion and hydrophilicity enhancement

make chitosan nanoparticles swell dramatically. By protonation of chitosan amino groups, the Schiff base bonding becomes instable and decomposition of the crosslinkers occurred. Therefore, by using such a reversible crosslinking reaction between chitosan and 2-chloro-3-formylquinoline and 3-formylquinolin-2(1*H*)-one, an interesting pHresponsive controlled release process can be achieved for acid-triggered burst release with the proposed nanoparticle. As shown in

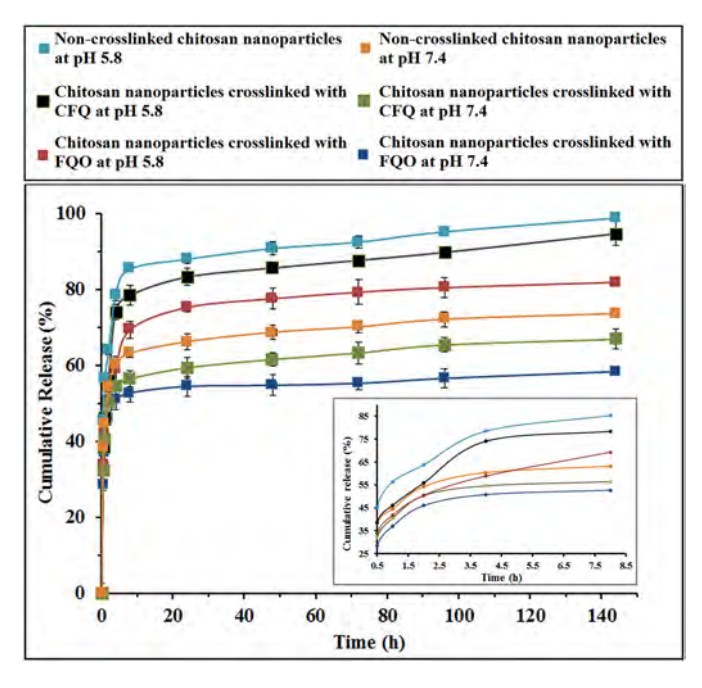


Fig. 7. In vitro release of quercetin from drug-loaded chitosan nanoparticles in PBS under different pH conditions (The inset shows the results for the first 10 h.)

**Table 2**Estimated values obtained by fitting the drug release data to the Higuchi and Korsmeyer–Peppas models.

Chitosan nanorods	pН	Higuchi		Korsmeyer–Peppas			Release mechanism
		k	r <sup>2</sup>	k'	r <sup>2</sup>	n	
Crosslinked with FQO	7.4	0.1866	0.8156	0.8109	0.9076	0.2213	Fickian diffusion
Crosslinked with CFQ		0.1735	0.7668	0.7974	0.9045	0.2060	Fickian diffusion
Non-crosslinked		0.1610	0.8795	0.8073	0.9546	0.1887	Fickian diffusion
Crosslinked with FQO		0.2017	0.9763	0.5040	0.9957	0.2568	Fickian diffusion
Crosslinked with CFQ	5.8	0.2116	0.9338	0.7334	0.9980	0.2598	Fickian diffusion
Non-crosslinked		0.1916	0.9470	0.7741	0.9816	0.2306	Fickian diffusion

Fig. 7, the burst release of chitosan nanoparticles crosslinked with FQO and CFQ is 69.3% and 78.4%, at pH 5.8 during the first 8 h, respectively. The quercetin release mechanism at this step could be illustrated by the quercetin diffusion localized at the surface of the chitosan–quinoline nanoparticles [45,46]. On the other hand, the cumulative release of chitosan–quinoline and chitosan–quinolone nanoparticles at pH 7.4 is 56.4% and 52.7% in first 8 h, respectively. After 150 h, whereas the drug release of chitosan nanoparticles crosslinked with CFQ was approximately completed at pH 5.8, only 82% of drug release occurred from chitosan nanoparticles crosslinked with FQO under similar condition. This could be explained by the stronger intermolecular hydrogen bonding between quercetin and FQO, which caused the lower release rate in comparison with chitosan nanoparticles crosslinked with CFQ.

Mechanism of drug release from crosslinked and non-crosslinked chitosan were analyzed at two pHs by Higuchi and Korsmeyer–Peppas equations and their data were listed in Table 2. Higuchi's release rate constant (k) and its correlation coefficient values ( $r^2$ ) were determined. The release data was also fitted into Korsmeyer–Peppas model and by considering release rate constants (k') and release constants (n), the fitting accuracy was calculated using correlation coefficient values ( $r^2$ ). When comparing these two models, the best fit method is Korsmeyer–Peppas, regarding to highest values of correlation coefficients, accordingly, the release mechanisms for all samples at both pHs are Fickian diffusion.

The SEM images of quercetin-loaded chitosan nanoparticles crosslinked with quinoline derivatives at pH 7.4 and 5.8 presented in

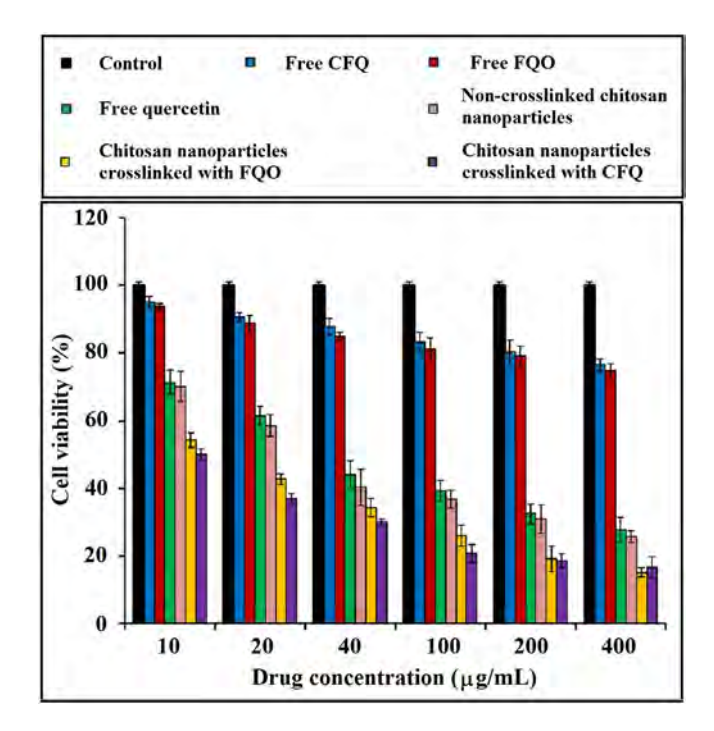


**Fig. 9.** Cell viability (%) of HeLa cancer cells after incubation with different quercetin formulations for 48 h.

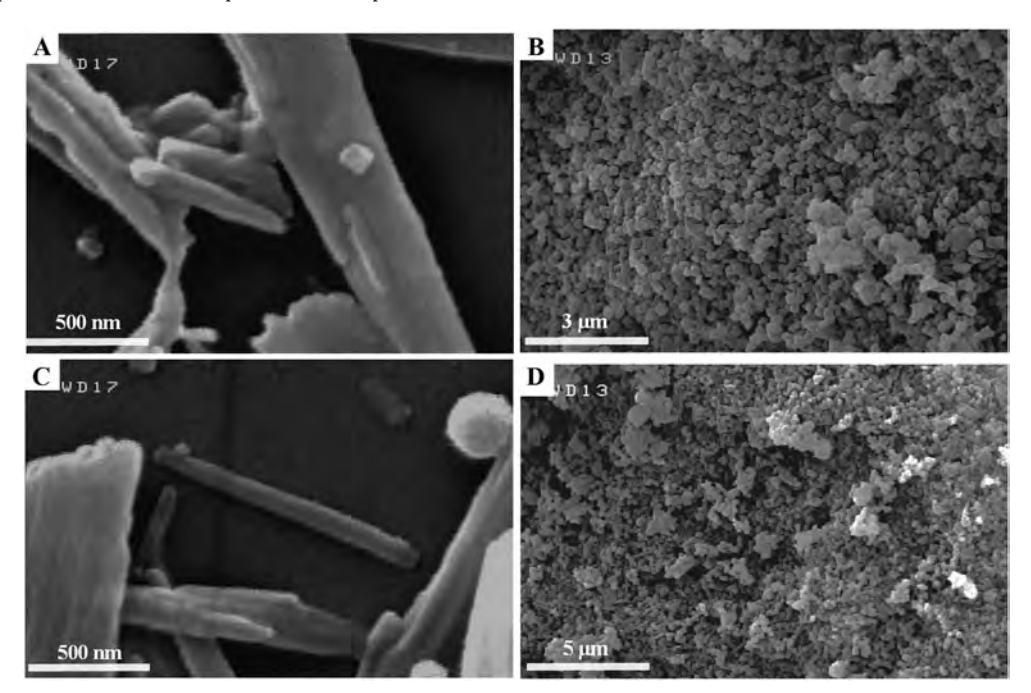


Fig. 8. SEM images of quercetin-loaded chitosan nanoparticles crosslinked with CFQ in pH 7.4 and 5.8 (A) and (B) respectively, quercetin-loaded chitosan nanoparticles crosslinked with FQO.

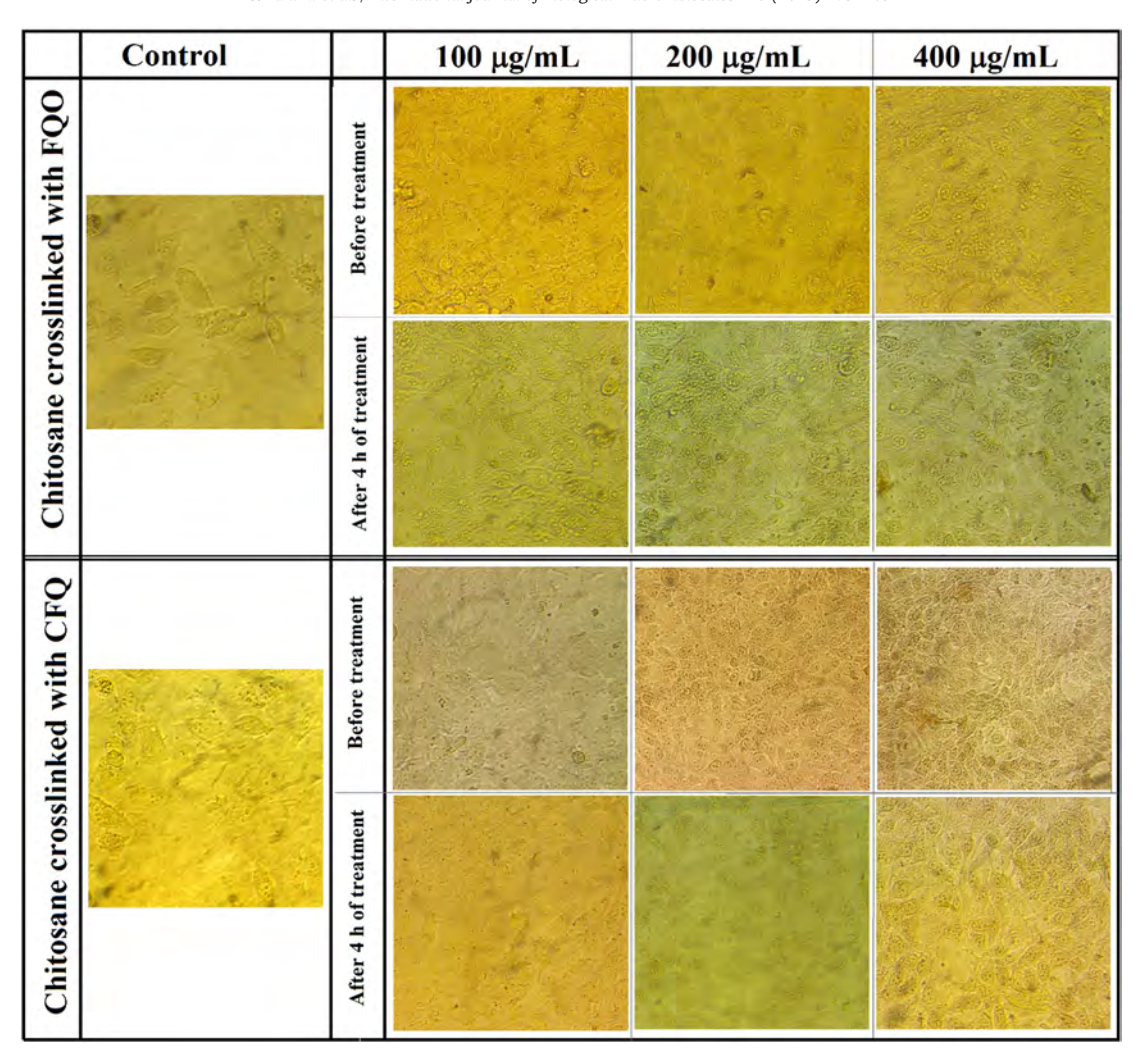


Fig. 10. Optical microscopy images of HeLa cells incubated with different concentrations of chitosan crosslinked with quinoline derivatives: before treatment and after 4 h of treatment.

Fig. 8. In neutral medium (pH 7.4), the quercetin–loaded chitosan nanoparticles crosslinked with quinoline derivatives maintain good nanorod shape and structural integrity, which promises that quercetin localized at the matrix of the chitosan–quinoline nanoparticles would not be released before reaching the tumor cells. While, in acidic medium (pH 5.8), the quercetin–loaded chitosan–quinoline nanoparticles have lost their nanorod shape and converted into tiny nanocubic crystals and consequently their disposal of the body is more easily. With the protonation of the chitosan amine groups at low pH, the imine bonds between the chitosan chains and quinoline molecules becomes weaken and instable, which led to decomposition of the crosslinked chitosan nanoparticles and quercetin was eventually released very rapidly. Therefore, by utilization of such a reversible crosslinking reaction between chitosan and quinoline derivatives, an interesting pH-sensitive controlled release system can be achieved.

# 3.3. Cell viability assays

MTT assay was used to evaluate the in vitro cytotoxicity of quercetin–loaded chitosan–quinoline nanoparticles, quercetin–loaded chitosan nanoparticles without of modification with quinoline derivatives, CFQ, FQO and the free quercetin at different concentrations from 10 to 400 µg mL<sup>-1</sup>, using HeLa cells as model. All the formulations exhibited remarkable anticancer activity against HeLa cells after 48 h incubation. As shown in Fig. 9, as the concentration of quercetin increased, the cell viability was further reduced. The half maximal inhibitory

concentration (IC50) value of the chitosan nanoparticles crosslinked with CFQ and FQO and free quercetin against HeLa cell lines were 10, 14 and about 32 µg mL<sup>-1</sup>, respectively. These results showed that quercetin-loaded chitosan-quinoline nanoparticles reveal higher cytotoxicity for cancer cell proliferation in comparison to that of free guercetin and quercetin-loaded chitosan nanoparticles without of modification with quinoline derivatives. Significantly, no remarkable difference was observed in cell viability between the quercetin-loaded chitosan nanoparticles crosslinked with quinoline derivatives during the experiment. Therefore, it can be concluded that chitosan-quinoline nanoparticles are able to enter the cells and show favorable pharmacological effect on cancer cells. Beside the anticancer activity of drug-loaded chitosan nanorods with two crosslinkers, the higher cell viability of non-crosslinked sample despite its higher drug release is interesting. In fact, after internalization of crosslinked nanoparticles by cancer cells, in the acidic media of lysosome and endosome the imine linkages of quinoline crosslinkers were quickly cleaved to protonated amino groups. This positive charge encourages nanoparticles to endosome/lysosome escape, which in turn provides the opportunity to increase system circulation efficiency and enhance favorable cellular and subcellular bioavailability [47].

Optical microscopy was employed to examine the influences of different concentration of two kinds of crosslinked chitosan nanoparticles on the morphology of HeLa cells. It can be seen from Fig. 10, that the cells which were incubated with drug-loaded nanorods even after 4 h incubation could change the spindle-like morphology of untreated cell (control cells) to rounded one. On the other hand, the images of HeLa

cells incubated with higher concentrations of NPs show an increase in internalization, the presence of nanoparticles inside the cells is the evidence of these phenomena. A homogeneous distribution of NPs inside the cells is also noteworthy.

#### 4. Conclusions

In summary, novel rod-like drug-loaded chitosan-quinoline nanoparticles were successfully designed and synthesized via an oil-inwater nanoemulsion method, using 2-chloro-3-formylquinoline and 3formylquinolin-2(1H)-one as friendly and non-toxic crosslinking agents. The structures of the obtained nanoparticles were carefully studied. The chitosan-quinoline nanoparticles were used as nanocarriers for efficient encapsulation of quercetin, exposing a pH-sensitive controllable release. The nanoparticles showed particle size in the range of 141–174 nm. The morphology of quercetin-loaded chitosan nanoparticles crosslinked with CFO and FOO was a monolithic structure with a kind of pattern and a regular nanorod shape, respectively. Due to the cleavage of crosslinked imine linkages present between chitosan and quinoline derivatives, the in vitro results displayed an accelerated drug release at lower pH condition in comparison to that occur under physiological conditions. Moreover, the in vitro quercetin release data showed that the chitosan nanoparticles crosslinked with FQO displayed a slow drug release in comparison to that of chitosan nanoparticles crosslinked with CFQ. In addition, the SEM images of quercetin-loaded chitosan nanoparticles crosslinked with quinoline derivatives in acidic medium exhibited that nanoparticles have lost their nanorod shape and converted into tiny nanocubic crystals, which led to decomposition of the crosslinked chitosan nanoparticles and quercetin was eventually released very rapidly. Compared to free quercetin, the quercetin-loaded chitosan-quinoline nanoparticles showed impressive comparable cytotoxicity against HeLa cells. Based on the obtained results, utilization of this new type of chitosan nanoparticles crosslinked with quinoline derivatives as potential drug delivery systems is concluded.

## Appendix A. Supplementary data

Supplementary data to this article can be found online at https://doi.org/10.1016/j.ijbiomac.2019.01.137.

## References

- M.R. Kumar, R.A. Muzzarelli, C. Muzzarelli, H. Sashiwa, A. Domb, Chitosan chemistry and pharmaceutical perspectives, Chem. Rev. 104 (2004) 6017–6084.
- [2] D. Depan, P.V. Surya, B. Girase, R. Misra, Organic/inorganic hybrid network structure nanocomposite scaffolds based on grafted chitosan for tissue engineering, Acta Biomater. 7 (2011) 2163–2175.
- [3] M. Diaconu, S.C. Litescu, G.L. Radu, Laccase–MWCNT–chitosan biosensor—a new tool for total polyphenolic content evaluation from in vitro cultivated plants, Sensors Actuators B Chem. 145 (2010) 800–806.
- [4] R. Jayakumar, D. Menon, K. Manzoor, S. Nair, H. Tamura, Biomedical applications of chitin and chitosan based nanomaterials—a short review, Carbohydr. Polym. 82 (2010) 227–232.
- [5] S.F. Peng, M.J. Yang, C.J. Su, H.L. Chen, P.W. Lee, M.C. Wei, H.W. Sung, Effects of incorporation of poly (γ-glutamic acid) in chitosan/DNA complex nanoparticles on cellular uptake and transfection efficiency, Biomaterials 30 (2009) 1797–1808.
- [6] Y.Q. Ye, F.L. Yang, F.Q. Hu, Y.Z. Du, H. Yuan, H.Y. Yu, Core-modified chitosan-based polymeric micelles for controlled release of doxorubicin, Int. J. Pharm. 352 (2008)
- [7] M. Thanou, J.C. Verhoef, H.E. Junginger, Oral drug absorption enhancement by chitosan and its derivatives, Adv. Drug Deliv. Rev. 52 (2001) 117–126.
- [8] Y.N. Fu, Y. Li, G. Li, L. Yang, Q. Yuan, L. Tao, X. Wang, Adaptive chitosan hollow microspheres as efficient drug carrier, Biomacromolecules 18 (2017) 2195–2204.
- [9] L. Liu, J.P. Yang, X.J. Ju, R. Xie, Y.M. Liu, W. Wang, J.J. Zhang, C.H. Niu, L.Y. Chu, Monodisperse core-shell chitosan microcapsules for pH-responsive burst release of hydrophobic drugs, Soft Matter 7 (2011) 4821–4827.
- [10] K. Gupta, F.H. Jabrail, Glutaraldehyde and glyoxal cross-linked chitosan microspheres for controlled delivery of centchroman, Carbohydr. Res. 341 (2006) 744–756.
- [11] A.P. Rokhade, N.B. Shelke, S.A. Patil, T.M. Aminabhavi, Novel interpenetrating polymer network microspheres of chitosan and methylcellulose for controlled release of theophylline, Carbohydr. Polym. 69 (2007) 678–687.

- [12] S. Rahimi, S. Khoee, M. Ghandi, Development of photo and pH dual crosslinked coumarin-containing chitosan nanoparticles for controlled drug release, Carbohydr. Polym. 201 (2018) 236–245.
- [13] M.M. Iftime, S. Morariu, L. Marin, Salicyl-imine-chitosan hydrogels: supramolecular architecturing as a crosslinking method toward multifunctional hydrogels, Carbohydr, Polym. 165 (2017) 39–50.
- [14] J.P. Michael, Quinoline, quinazoline and acridone alkaloids, Nat. Prod. Rep. 16 (1999) 697–709.
- [15] C.W. Wright, J. Addae-Kyereme, A.G. Breen, J.E. Brown, M.F. Cox, S.L. Croft, Y. Gökçek, H. Kendrick, R.M. Phillips, P.L. Pollet, Synthesis and evaluation of cryptolepine analogues for their potential as new antimalarial agents, J. Med. Chem. 44 (2001) 3187–3194
- [16] S. Cretton, S. Dorsaz, A. Azzollini, Q. Favre-Godal, L. Marcourt, S.N. Ebrahimi, F. Voinesco, E. Michellod, D. Sanglard, K. Gindro, J.L. Wolfender, M. Cuendet, P. Christen, Antifungal quinoline alkaloids from Waltheria indica, J. Nat. Prod. 79 (2016) 300–307.
- [17] M. Alam, M. Shaharyar, H. Hamid, S. Nazreen, S. Haider, M.S. Alam, Synthesis of novel 8-hydroxy quinolin based 1, 3, 4-oxadiazoles and S-substituted 1, 2, 4triazole derivatives and evaluation of their anti-inflammatory, analgesic, ulcerogenic and anti-microbial activities, Med. Chem. 7 (2011) 663–673.
- [18] R.E. Khidre, B.F. Abdel-Wahab, F.A. Badria, New quinoline-based compounds for analgesic and anti-inflammatory evaluation, Lett. Drug Des. Discovery 8 (2011) 640–648.
- [19] S. Vandekerckhove, M. D'hooghe, Quinoline-based antimalarial hybrid compounds, Bioorg. Med. Chem. 23 (2015) 5098–5119.
- [20] K. Plevová, K. Briestenská, F. Colobert, J. Mistríková, V. Milata, F.R. Leroux, Synthesis and biological evaluation of new nucleosides derived from trifluoromethoxy-4quinolones, Tetrahedron Lett. 56 (2015) 5112–5115.
- [21] A. Kamal, R. Abdul, S. Riyaz, Y. Poornachandra, B. Moku, C.G. Kumar, S.M. Hussaini, B. Sridhar, P.K. Machiraju, Regioselective synthesis, antimicrobial evaluation and theoretical studies of 2-styryl quinolines, Org. Biomol. Chem. 13 (2015) 1347–1357.
- [22] Y. Parthasaradhi, S. Suresh, B.R. Kumar, T.S. Jyostna, Design and synthesis of some new quinoline based 1, 2, 3-triazoles as antimicrobial and antimalarial agents, orbital: the electronic, J. Chem. 7 (2015) 264–269.
- [23] O. Afzal, S. Kumar, M.R. Haider, M.R. Ali, R. Kumar, M. Jaggi, S. Bawa, A review on anticancer potential of bioactive heterocycle quinoline, Eur. J. Med. Chem. 97 (2015) 871–910.
- [24] D.A. Ibrahim, D.A.A. El Ella, A.M. El-Motwally, R.M. Aly, Molecular design and synthesis of certain new quinoline derivatives having potential anticancer activity, Eur. J. Med. Chem. 102 (2015) 115–131.
- [25] R.S. Gonçalves, C.R. Kaiser, M.C. Lourenço, M.V. de Souza, J.L. Wardell, S.M. Wardell, A.D. Da Silva, Synthesis and antitubercular activity of new mefloquine-oxazolidine derivatives, Eur. J. Med. Chem. 45 (2010) 6095–6100.
- [26] M.H. Gelb, Drug discovery for malaria: a very challenging and timely endeavor, Curr. Opin. Chem. Biol. 11 (2007) 440–445.
- [27] D.S. Ongarora, J. Gut, P.J. Rosenthal, C.M. Masimirembwa, K. Chibale, Benzoheterocyclic amodiaquine analogues with potent antiplasmodial activity: synthesis and pharmacological evaluation, Bioorg. Med. Chem. Lett. 22 (2012) 5046–5050.
- [28] N. Sharma, D. Mohanakrishnan, U.K. Sharma, R. Kumar, A.K. Sinha, D. Sahal, Design, economical synthesis and antiplasmodial evaluation of vanillin derived allylated chalcones and their marked synergism with artemisinin against chloroquine resistant strains of Plasmodium falciparum, Eur. J. Med. Chem. 79 (2014) 350–368.
- [29] R. Abonia, D. Insuasty, J. Castillo, B. Insuasty, J. Quiroga, M. Nogueras, J. Cobo, Synthesis of novel quinoline-2-one based chalcones of potential anti-tumor activity, Eur. J. Med. Chem. 57 (2012) 29–40.
- [30] M.K. Singh, A. Chandra, B. Singh, R.M. Singh, Synthesis of diastereomeric 2, 4-disubstituted pyrano [2, 3-b] quinolines from 3-formyl-2-quinolones through O—C bond formation via intramolecular electrophilic cyclization, Tetrahedron Lett. 48 (2007) 5987–5990.
- [31] T. Higuchi, Mechanism of sustained-action medication. Theoretical analysis of rate of release of solid drugs dispersed in solid matrices, J. Pharm. Sci. 52 (1963) 1145–1149.
- [32] R.W. Korsmeyer, R. Gurny, E. Doelker, P. Buri, N.A. Peppas, Mechanisms of solute release from porous hydrophilic polymers, Int. J. Pharm. 15 (1983) 25–35.
- [33] M. Ghandi, S. Rahimi, N. Zarezadeh, Synthesis of novel tetrazole containing quinoline and 2, 3, 4, 9-tetrahydro-1H-β-carboline derivatives, J. Heterocyclic Chem. 54 (2017) 102–109.
- [34] H. Chen, X. Hu, E. Chen, S. Wu, D.J. McClements, S. Liu, B. Li, B. Li, Preparation, characterization, and properties of chitosan films with cinnamaldehyde nanoemulsions, Food Hydrocoll. 61 (2016) 662–671.
- [35] S. Kumar, J. Koh, Physiochemical, circular dichroism-induced helical conformation and optical property of chitosan azo-based amino methanesulfonate complex, J. Appl. Polym. Sci. 124 (2012) 4897–4903.
- [36] S. Hirano, K. Nagamura, M. Zhang, S.K. Kim, B.G. Chung, M. Yoshikawa, T. Midorikawa, Chitosan staple fibers and their chemical modification with some aldehydes, Carbohydr. Polym. 38 (1999) 293–298.
- [37] S. Noppakundilograt, P. Buranagul, W. Graisuwan, C. Koopipat, S. Kiatkamjornwong, Modified chitosan pretreatment of polyester fabric for printing by ink jet ink, Carbohydr, Polym. 82 (2010) 1124–1135.
- [38] C. Demetgül, N. Beyazit, Synthesis, characterization and antioxidant activity of chitosan-chromone derivatives, Carbohydr. Polym. 181 (2018) 812–817.
- [39] M.A. Pujana, L. Pérez-Álvarez, L.C.C. Iturbe, I. Katime, Biodegradable chitosan nanogels crosslinked with genipin, Carbohydr. Polym. 94 (2013) 836–842.

- [40] P. Sorlier, C. Rochas, I. Morfin, C. Viton, A. Domard, Light scattering studies of the solution properties of chitosans of varying degrees of acetylation, Biomacromolecules 4 (2003) 1034–1040.
- [41] S. Kumar, J. Koh, H. Kim, M. Gupta, P. Dutta, A new chitosan-thymine conjugate: synthesis, characterization and biological activity, Int. J. Biol. Macromol. 50 (2012) 403, 502
- [42] H. Du, M. Liu, X. Yang, G. Zhai, The role of glycyrrhetinic acid modification on preparation and evaluation of quercetin-loaded chitosan-based self-aggregates, J. Colloid Interface Sci. 460 (2015) 87–96.
- [43] M.P. Souza, A.F.M. Vaz, M.T.S. Correia, M.A. Cerqueira, A.A. Vicente, M.G. Carneiro-da-Cunha, Quercetin-loaded lecithin/chitosan nanoparticles for functional food applications, Food Bioprocess Technol. 7 (2014) 1149–1159.
- [44] W. Nan, L. Ding, H. Chen, F.U. Khan, L. Yu, X. Sui, X. Shi, Topical use of quercetin-loaded chitosan nanoparticles against ultraviolet B radiation, Front. Pharmacol. 9 (2018) 826.
- [45] A. Jain, K. Thakur, P. Kush, U.K. Jain, Docetaxel loaded chitosan nanoparticles: formulation, characterization and cytotoxicity studies, Int. J. Biol. Macromol. 69 (2014) 546–553.
- [46] R. Yoksan, J. Jirawutthiwongchai, K. Arpo, Encapsulation of ascorbyl palmitate in chitosan nanoparticles by oil-in-water emulsion and ionic gelation processes, Colloids Surf. B: Biointerfaces 76 (2010) 292–297.
- [47] A. Paillard, F. Hindré, C. Vignes-Colombeix, J.P. Benoit, E. Garcion, The importance of endo-lysosomal escape with lipid nanocapsules for drug subcellular bioavailability, Biomaterials 31 (2010) 7542–7554.